ELSEVIER

Journal of Chromatography A, 816 (1998) 145–158

JOURNAL OF CHROMATOGRAPHY A

Characterization of hematite and its interaction with humic material using flow field-flow fractionation

Mark P. Petteys, Martin E. Schimpf*

Department of Chemistry, Boise State University, Boise, ID 83725, USA

Received 21 March 1998; received in revised form 22 May 1998; accepted 27 May 1998

Abstract

The ability of flow field-flow fractionation (FlFFF) to characterize the interaction of organic matter with mineral colloids is demonstrated. Colloidal hematite is first prepared and the size distribution is characterized by scanning electron microscopy, FlFFF, and multi-angle light scattering (MALS). Next, the interaction of well-characterized humic and fulvic acids with the colloidal hematite is studied by separating and quantifying the adsorbed and free acids using FlFFF. Both kinetic and thermodynamic information is obtained, including adsorption isotherms. The adsorptive capacity of hematite is greater for humic acid compared to fulvic acid, probably due to the formation of multiple adsorption layers.

Keywords: Flow field-flow fractination; Field-field fractionation; Adsorption isotherms; Hematite; Humic acid; Fulvic acid

1. Introduction

Humic and fulvic acids (humics) formed from the oxidative degradation of plant matter are very active in the formation and transport of material throughout the environment. In the weathering of rocks, for example, humics are carried into cracks by rainwater or snow melt and subsequently enhance the breakdown of rock to secondary minerals such as clays and metal oxides. Humics also bind hydrophobic organic compounds (HOC), including many pollutants. The binding of HOC to acids can increase their transport through the subsurface environment. However, humics themselves bind to a variety of silicates and metal oxides. Thus, dissolved humics can form organic coatings on aquifer sediments, which therefore facilitate the sorption of HOC. As a result, HOC can be transported through one environment only to be re-deposited in another as conditions change.

Unfortunately, comprehensive information is lacking on the complexation of humics by the major oxides of iron, which are the most abundant minerals in the environment. Nayak et al. [1] reported that adsorption of humics to colloidal iron oxides decrease with increasing acid content in the acid. However, adsorption increases as the pH is reduced [2]. These two observations are consistent with a mechanism that involves ligand exchange of acid groups in the acid with water or hydroxide-groups at the mineral surface, a process that is inhibited by repulsive forces between molecules with high charge densities. The ligand-exchange mechanism has been supported by other studies. For example, Varacachari et al. [3] demonstrated that humic acid adsorption increases with the addition of salt, presumably due to

*Corresponding author.

0021-9673/98/$19.00
PII: S0021-9673(98)00476-2

shielding of the repulsive forces between carboxylate groups as a result of cation-exchange.

Murphy et al. [4] proposed conformational changes in the adsorption of humic acids to mineral colloids. The rearrangement of humic acids under changing conditions is also indicated in the work of Engebretson et al. [5], who found that interactions between pyrene and humic acid increases with ionic strength. In that work, pyrene fluorescence was shown to actually increase in the presence of bromide salts, which are known quenching agents [6,7], provided humic acid is present. The protection of pyrene from fluorescence quenching by humic acid is strong evidence that pyrene is incorporated into humic acid structures which form only in the presence of cations. We recently obtained direct evidence for conformational rearrangements in humic acids with subtle changes in pH and ionic strength by measuring dramatic changes in hydrodynamic diameters using flow field-flow fractionation (FlFFF) [8].

While our comprehension of humic and fulvic acid behavior continues to increase, a complete understanding of the role that adsorption complexes play in the transport of pollutants requires that adsorption be studied under a wide range of conditions. Typically, adsorption isotherms are established by equilibrating the adsorbate with support material for a specified amount of time, then separating the free adsorbate by centrifugation, followed by analysis of the supernatant. Colloidal-sized particles are difficult to centrifuge without an ultracentrifuge, and the large fields required can distort the adsorption equilibrium, particularly in systems where adsorption is a dynamic and reversible process. When the centrifugal field is relaxed, partial remixing can occur in submicron-sized systems, which undergo rapid diffusion. Studies of humic adsorption to mineral colloids are especially difficult because both materials have significant diffusion coefficients. In this paper we present FlFFF as an effective alternative to traditional methods for the study of adsorption complexes.

FlFFF is one of several subtechniques in the FFF family of techniques that are used to separate and characterize macromolecules, colloids, and particulate materials through the application of an external field, which results in the retardation of material moving through a ribbon-shaped channel. Historically, FFF has been limited primarily to materials having molecular weights above a few thousand. The retention of smaller materials in the FFF channel is not adequate to induce separation. In 1987, Berthod and Armstrong [9] proposed the use of secondary chemical equilibria (SCE) to expand the application of FFF to lower molecular weight materials. In SCE–FFF, the smaller analyte material is retained by associating it with a larger mediating agent, which itself is retained in the FFF channel. The separation of components is therefore based on differences in their interaction with the mediating agent. At the time SCE was proposed as a method to increase the versatility of FFF, it had already been used to expand other analytical separation techniques. For example, micelle-forming surfactants that interact with solutes are used to enhance retention in HPLC, and to separate uncharged solutes in micellar electrokinetic capillary chromatography [10].

In their initial paper on SCE–FFF [9], Berthod and Armstrong developed a model for predicting analyte retention when the mediating agent (additive) is placed in the carrier-liquid reservoir, so that it is pumped continuously through the channel. The model is based on the partitioning of analyte between the bulk liquid and the additive, which itself is nonuniformly distributed in the channel due to its interaction with the applied field. An equation was derived that relates analyte retention directly to the volume fraction of additive in the carrier liquid, its retention in the channel, and to the partition coefficient, which quantifies the equilibrium distribution of the analyte between the additive and the bulk liquid. The model was later refined and expanded by Hoyos and Martin [11] in an effort to broaden the range of conditions to which it could be applied.

Despite numerous examples in chromatography demonstrating the utility of SCE, there is only one report on the use of SCE to separate small molecules by FFF [12]. However, independent reports from the laboratories of Caldwell [13] and Giddings [14] have demonstrated a separation mechanism related to that of FFF–SCE. In those reports, the retention of macromolecules was increased by adsorption to particulate matter in sedimentation FFF channels. Since the materials in those reports were adsorbed irreversibly, the support did not need to be pumped continuously through the channel, rather it was equilibrated with the adsorbate prior to injection. By

comparing the retention level of the support in the presence and absence of adsorbate, the mass of the adsorption layer was determined.

In the work reported here, we use FlFFF to characterize the adsorption of two different acids to hematite. One of these materials is classified as a humic acid and the other a fulvic acid. Compared to centrifugation, FFF separations are faster because differential displacement across the field occurs over a distance on the order of micrometers, as opposed to centimeters in centrifugation. By coupling that differential displacement with a nonuniform flow profile, material that is adsorbed to colloidal-sized particles can be separated from the non-adsorbed material in a few minutes. An additional advantage of the fast separation time is that information on the kinetics of adsorption can be obtained on systems that reach equilibrium in a relatively short period of time. Furthermore, only milligram quantities of material are required to run the necessary experiments for characterizing an adsorption complex.

In the method described in this work, humic or fulvic acid is mixed with hematite (Fe_2O_3) and allowed to equilibrate for a specific amount of time before being injected into the channel. Acids that are not adsorbed to hematite at the time of injection elute in the void volume of the channel. Acids that are adsorbed to the hematite are retained because the hematite is retained. Although some desorption may occur as the complex is diluted in the channel, the process is slow enough that even desorbed acids are somewhat retained and therefore separated from those acids that were not adsorbed to hematite at the time of injection. This is important because it allows thermodynamic information on adsorption to be obtained without pumping the support continuously through the channel. Continuous infusion of hematite would lead to rapid deterioration of the channel and a subsequent loss of quantitative information. The deterioration of a FlFFF channel by continuous infusion of hematite would be especially rapid due to the susceptibility of the membrane to fouling. Sedimentation FFF may be a viable alternative but is not available in our laboratory.

The retention time of adsorbed material increases with the stability of the adsorption complex because when the material desorbs, it diffuses into faster moving flowstreams. As it moves ahead of the hematite, chances for re-adsorption diminish. In the work reported here, the retention of acid increases with equilibration time (the time between mixing and injection). By monitoring that increase, we can study and compare the stability of different adsorption complexes.

Beyond a given equilibration time, retention of the acids studied in this work reached a plateau value; the threshold equilibration time is different for each acid. Once the threshold time is established, we can use a fixed equilibration time (greater than the threshold value) to obtain thermodynamic information. For example, we can quantify the amount of acid adsorbed at the time of injection by measuring the areas of both retained and unretained peaks in the elution profiles. By making such measurements for different amounts of each acid mixed with a fixed amount of hematite, we can establish adsorption isotherms. The method requires two assumptions: (1) adsorbed acid is not desorbed during the stop-flow relaxation period, and (2) the recovery of the acid that is not adsorbed at the time of injection is either complete, or remains the same regardless of the presence or absence of hematite in the injected sample. The experimental results indicate that both assumptions are reasonable.

2. Materials and methods

2.1. Acids

Humic acid is distinguished from fulvic acid by its precipitation from an aqueous solution when the pH is lowered to a value of 1. Suwannee River fulvic acid (SRFA) was obtained in lyophilized form from the International Humic Substances Society; it is widely used and well-characterized. A sphagnum-peat humic acid (SPHA) was isolated by Robert Wershaw (US Geological Survey; Denver, CO, USA) from Thoreau's Bog near Boston, MA (USA). The humic acids were extracted from the matrix material with a 0.1 *M* NaOH solution. The precipitate formed by lowering the pH to 1 with HCl was separated from the supernatant by centrifugation and washed three times with DI water. Next, the humic acids were re-dissolved by adding just enough 0.1 *M* NaOH. The resulting solution, which had a pH of 8,

was then lyophilized. In our study of their adsorption to hematite, the humic samples were first dissolved in DI water at various concentrations. These solutions were then mixed with hematite suspensions in a 1:1 volume ratio.

The molecular weight and size distributions of both humic samples were characterized by FlFFF in a previous study [8]. Molecular weight analysis depends on the use of calibration standards. Sulfonated polystyrene is the standard typically used, but molecular weights calculated using this standard vary with the pH and ionic strength of the carrier liquid, whether FFF or size exclusion chromatography (SEC) is used [15]. We have found that a dilute solution of NaOH (pH 8.5) gives good separations and unimodal distributions. This carrier liquid also yields molecular weight values for the fulvic acid consistent with those previously reported by Beckett et al. [16], who confirmed FlFFF data with vapor-phase osmometry and X-ray diffraction data.

In contrast to molecular weight distributions, FlFFF yields distributions of the hydrodynamic radius directly from elution profiles without calibration. The size distributions in NaOH solutions at pH 8.5 are fairly narrow, although a small amount of larger (perhaps aggregated) material is evidenced by a long tail in the distribution. Values of the molecular weight and hydrodynamic radius associated with the peak of their respective distributions (M_P and $r_{h,P}$, respectively) for SPHA and SRFA are summarized in Table 1. Both M_P and $r_{h,P}$ are smaller in the fulvic acid. Table 1 also lists the UV absorption coefficients for both materials measured at 280 nm (a_{280}). Since aromatic groups strongly absorb radiation at 280 nm, a higher value of a_{280} indicates a more hydrophobic molecule. Thus, the fulvic acids is only slightly more hydrophobic than the humic acid; differences in size or molecular weight are more significant.

Table 1
Summary of information on acids

	M_P (g mol^{-1})	$r_{h,P}$ (nm)	a_{280} (l g^{-1} cm^{-1})
SPHA	1630	1.9	13.6
SRFA	980	0.9_3	15.0

2.2. Preparation of colloidal hematite

Colloidal hematite (Fe_2O_3) was prepared using a procedure first described by Matijevic and Scheiner [17], later modified by Penners and Koopal [18], and finally modified in our laboratory. The procedure converts iron (III) chloride to hematite by the following reaction

$$2FeCl_3 + 3H_2O \rightarrow Fe_2O_3(s) + 6H^+ + 6Cl^-$$

The size and morphology of the resulting iron oxide is controlled by temperature and reaction time, as well as the quantity of HCl added to the reaction mixture. For the work reported here, the following procedure was used: (1) 2.9 g $FeCl_3$ was dissolved in 25 ml of deionized (DI) water; 8 μl of concentrated HCl was added to the resulting solution (A). (2) A separate solution (B) was prepared by adding 300 μl of concentrated HCl to 975 ml of DI water in a 2-l round-bottom flask. (3) Solution A was vacuum filtered through a 0.2 μm filter while solution B was heated to 100°C. (4) Solution A was added to solution B while stirring vigorously with a magnetic stirrer. (5) The mixture was covered with a watch-glass and placed in a convection oven at 100°C for 24 h. (6) The resulting suspension was cooled to room temperature and 30 ml aliquots were centrifuged at 15 000 rpm for 30–40 min. (7) The supernatant was discarded and the remaining reddish-brown particles were resuspended in DI water with one h of sonication. Centrifugation and resuspension was repeated twice, raising the pH of the suspension from 1.5 to 2.5. The resulting colloidal suspension was stable for more than 7 months.

For the adsorption experiments, 30 ml aliquots of the hematite suspension were repeatedly centrifuged and resuspended in DI water until the pH was raised to 7. Raising the pH resulted in only a minor amount of additional precipitation. In fact, precipitation at the higher pH was limited to a coat of hematite on the glass surface of the containment vessel. Based on this observation, we used 20-ml plastic vials for the adsorption experiments.

We examined the hematite at different points in time with a Model JSM-T300 scanning electron microscope from Jeol, Corp. (Tokyo, Japan). To prepare the sample for imaging, one drop of the hematite suspension was placed on a glass cover slide, the solvent was allowed to dry, and residue silver-sputtered.

2.3. 2.3. FlFFF instrumentation

Two Model F-1000 FlFFF instruments from FFFractionation, Inc. (Salt Lake City, UT, USA) were used in this work. The channel in both instruments has a breadth of 2.5 cm and a tip-to-tip length of 29.5 cm. The channel in instrument A has a nominal thickness of 0.013 cm. However, the actual thickness varies with the carrier-liquid, presumably due to swelling of the membrane. We used two different carrier liquids in this work: DI water and a DI water solution containing FL-70 surfactant (0.05 vol%) from Fisher Scientific (Pittsburgh, PA, USA) and NaN_3 (0.02 wt%) from Aldrich Chemical Co. (Milwaukee, WI, USA). In DI water, very little swelling occurs and the channel thickness is governed by the thickness of the polyester spacer (0.0127 cm) used to form the channel; the resulting void volume is 0.90 ml. When FL-70 surfactant is added to the carrier liquid, the channel thickness is reduced. Based on the elution of an unretained polystyrene sulfonate standard, the reduced thickness is 0.010 cm; the resulting void volume is 0.70 ml. The accumulation wall membrane in instrument A is made of cellulose acetate and has a nominal molecular weight cutoff (MWCO) of 1000 $g\,mol^{-1}$, as determined by the manufacturer using proteins. For acids, however, the effective molecular weight cutoff is 600 $g\,mol^{-1}$ [8]. Carrier liquid was delivered to instrument A using two Model 590 pumps from Waters Corp. (Milford, MA, USA). Detection was achieved with an Alltech (Deerfield, IL, USA) Model 200 variable-wavelength UV detector. The detector signal was digitized and collected by a Waters Corp. Maxima 820 Chromatography Workstation. The signal was also sent to a chart recorder for visual display of the elution profile.

Instrument B was used to fractionate the hematite sample for characterization by a Dawn DSP multi-angle laser light scattering (MALS) instrument from Wyatt Technology (Santa Barbara, CA, USA). The channel membrane is made of regenerated cellulose and has a nominal molecular weight cutoff of 10 000 $g\,mol^{-1}$. The channel spacer is 0.0254 cm thick and the measured void volume is 1.30 ml. Axial flow to instrument B was provided by a Ministar K-500 dual-piston pump from Knauer (Berlin, Germany). Crossflow was sustained with a Model P-500 syringe pump from Pharmacia Biotech, Inc. (Piscataway, NJ, USA). The inlet to the crossflow pump was attached to the channel-crossflow outlet, thereby re-circulating the crossflow in a continuous loop. Carrier liquid was pre-filtered through 0.1 μm diameter filter paper using a vacuum pump. In addition, manifold filters (0.025 μm) were placed between both pumps and the corresponding channel inlets in order to trap additional particulate material. The light scattering signals, which are digitized by the MALS instrument, were processed by Astra® software using a desktop computer.

A stop-flow procedure was used for sample relaxation. In this procedure, axial flow is routed around the channel for 110 s after sample injection while crossflow is maintained. During the stop-flow period, 1.0–1.3 channel volumes (depending on the channel thickness) of crossflow relax the sample into its steady-state concentration profile at the accumulation wall.

2.4. Hematite size distribution

A FlFFF elution profile can be converted into a size distribution when the dependence of retention on particle size is known. The dependence can be established by one of two methods. The first method [19] utilizes the following relationship between the fundamental retention parameter λ and the hydrodynamic radius (r_h) of an eluting particle:

$$\lambda = \frac{kTV^0}{6w^2\pi\eta V_c} 1r_h \tag{1}$$

where k is Boltzmann's constant, T is absolute temperature, V^0 is the geometric volume of the channel, η is the carrier-liquid viscosity, and V_c is the rate of crossflow. Parameter λ is calculated from the time (t_r) or volume (V_r) of carrier liquid required to flush a component through the channel:

$$R = t^0/t_r = V^0/V_r = 6\lambda[\coth(1/2\lambda) - 2\lambda] \tag{2}$$

Here, t^0 is the retention time of a component that is not affected by the field and R is termed the retention ratio. By combining Eqs. (1) and (2), each digitized value of V_r (or t_r) in an elution profile has an associated hydrodynamic radius. The second method for relating particle size to its retention in the FlFFF

channel is based on calibration with particle standards of known diameter [20]; in this work, we calibrated the channel with polystyrene latex particles from Polysciences, Inc. (Warrington, PA, USA).

Utilizing the dependence of retention on particle size, the FlFFF elution profile is transformed directly into a size distribution. When a UV detector is used, we assume that the response of the detector is related to the mass-based concentration of particles in the eluting stream, while being independent of the particle size. Due to Mie scattering, which causes larger particles to scatter more light, detector response is not strictly independent of particle size [21]. However, such effects are negligible for the small particles examined in this work [22]. A detailed discussion of the conversion of elution profiles into size distributions can be found in reference [23].

With the MALS instrument, particle size is calculated using the Rayleigh-Gans approximation, which relates the excess Rayleigh ratio $R(\theta)$ to the scattering form factor $P(\theta)$ as follows [24]:

$$R(\theta) = K^{*}cMP(\theta) \tag{3}$$

Here K^* is an optical constant, c is sample concentration, and M is molar mass. $R(\theta)$ is directly related to the amount of light scattered in excess of that due to the solvent, while $P(\theta)$ is related to the root mean square radius ($<r^2>^{1/2}$) by

$$P(\theta) = 1 - a_1[2k\sin(\theta/2)]^2 + a_2[2k\sin(\theta/2)]^4 - \ldots \tag{4}$$

where

$$a_1 = \frac{1}{3} <r^2>^{1/2} = \frac{1}{3M}\int r^2 \, \mathrm{d}M \tag{5}$$

Parameter r is the distance between the center of gravity and each mass element in the particle. By ratioing $R(\theta)/K^*c$ to R/K^*c at a fixed angle (such as 90°), the term K^*c in Eq. (3) cancels, and a plot of the ratio against $\sin^2(\theta/2)$ yields $<r^2>^{1/2}$ without prior knowledge of c or K^*.

The Rayleigh-Gans theory assumes that the incident light wave is unaffected by the scattering particle, which is strictly true only when the refractive index (n) of the particle equals that of the surrounding medium (n_o). In practice, the Rayleigh-Gans theory works well if the difference in refractive index is not too large. For example, Thielking et al. [25] found that size measurements of submicron-sized polystyrene spheres ($n = 1.59$) in aqueous suspensions ($n_0 = 1.33$) agreed well with those obtained by transmission electron microscopy.

3. Results and discussion

3.1. Characterization of hematite

The hematite was evaluated by several methods. First, scanning electron microscopy (SEM) was used to identify the general size and shape characteristics. The particles are generally spherical and have a narrow size distribution, as illustrated in Fig. 1. A statistical analysis of 100 particles by SEM yielded an average radius of 41 nm with a standard deviation of 5 nm.

Next, FlFFF (instrument A) was used to separate the hematite and obtain a detailed size distribution. In Fig. 2A the elution profile obtained from a freshly prepared hematite sample before the pH of the sample was raised to 7 by the rinsing procedure discussed above is shown. The carrier liquid was DI water containing 0.05 vol% Fl-70 and 0.02 wt% NaN_3. The surfactant is added to improve peak shape by reducing the interaction of particles with each other and with the accumulation-wall membrane; NaN_3 is added as a bacteriocide. The detector was set at 260 nm, which gave the best signal-to-noise ratio for hematite detection. For converting the elution profile into a size distribution, we compared both methods discussed above for establishing the dependence of V_r on r_h. In the first method, Eqs. (1) and (2) were used with a temperature of 294 K and a viscosity of 0.955 cP. In the second method, four monodisperse polystyrene latex colloids were used to obtain the following relationship between r_h and V_r:

$$r_h = 15.125V_r - 7.625 \quad (r = 0.999) \tag{6}$$

The resulting size distributions are displayed in Fig. 2B. They have a similar shape but are shifted from one another along the size axis by 2 nm. Thus, the distribution peaks at an r_h value of 41 nm when

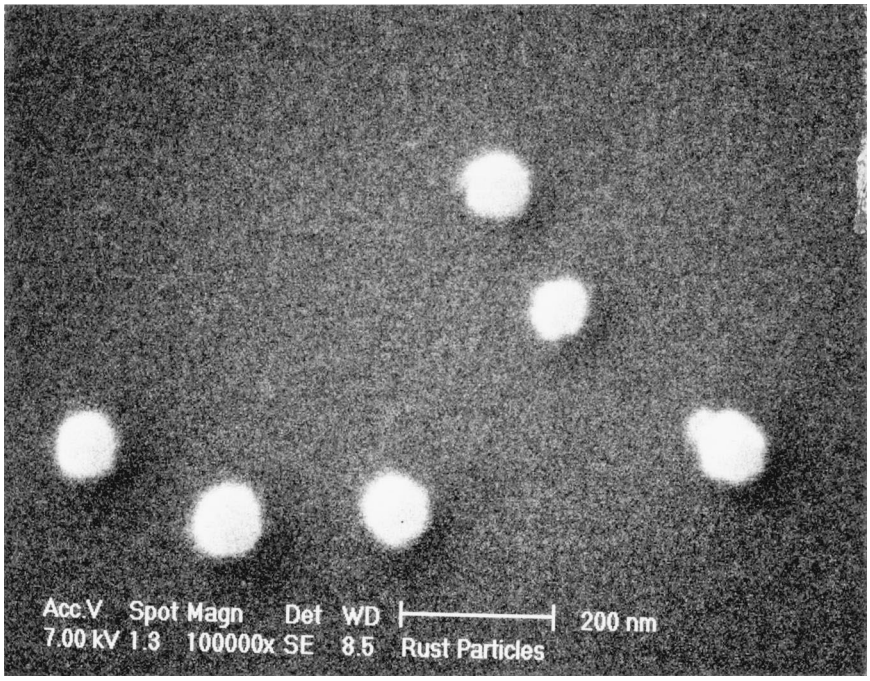

Fig. 1. Scanning electron micrograph of colloidal hematite.

retention theory is used to establish the relationship between V_r and r_h, but when calibration with latex standards is used, the distribution peaks at an r_h value of 43 nm. Based on repeated injections, the standard deviation of the r_h value associated with the peak of the size distribution ($r_{h,p}$) is 1 nm, regardless of the method used to establish the relationship between V_r and r_h. Regression statistics on the data used to establish Eq. (6) indicate a standard uncertainty in calculated $r_{h,p}$ values of 5 nm. Therefore, the discrepancy between the two distributions illustrated in Fig. 2B lies within the experimental uncertainty.

The hematite suspension was re-analyzed by instrument A after raising the pH of the suspension to 7. Comparing the hematite size distributions before and after raising the pH showed no significant differences, even after 7 months.

From the digitized data used to plot the size distributions, the standard deviation of the distribution was calculated to be 13 nm, which is significantly greater than the value of 5 nm estimated by SEM. The discrepancy is due to band broadening of the elution profile, which was not removed before transformation of the elution profiles into size distributions.

The hematite was analyzed by a third method that combines FlFFF (instrument B) with MALS detection. With this configuration, particle size is measured directly as the material elutes from the channel. A plot of the root-mean-square radius ($<r^2>^{1/2}$) of the particles as a function of V_r is superimposed on the elution profile in Fig. 3A. The resolving power of the FlFFF instrument is demonstrated by the increase in $<r^2>^{1/2}$ with V_r. Fig. 3B illustrates the weight-fraction size distribution calculated from the light scattering data. The value of $<r^2>^{1/2}$ associated with the peak of the distribution ($<r^2>_p^{1/2}$) is 36.5 nm and the standard deviation in $<r^2>^{1/2}$ is 6 nm.

In order to analyze the consistency of the size distributions illustrated in Figs. 2 and 3, we must know the relationship between r_h and $<r^2>^{1/2}$, which requires the shape and morphology of the

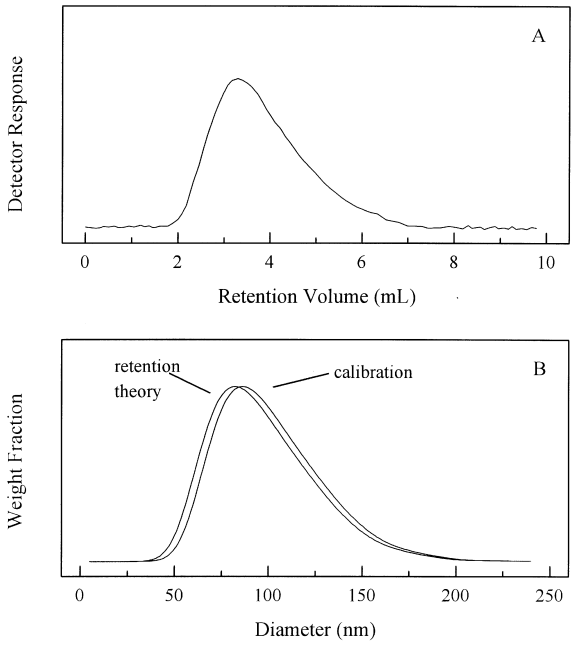

Fig. 2. FlFFF elution profile of hematite (A) and a comparison of size distributions obtained by relating retention time to hydrodynamic radius using latex standards versus retention theory (B). The aqueous carrier liquid contains 0.05 vol% FL-70 and 0.02 wt% NaN_3.

particles to be known. For perfect spheres with a solid core, the relationship between these two size parameters is

$$<r^2>^{1/2} = 0.775 r_h \text{ solid spheres} \quad (7)$$

For other particles, the multiplication factor varies between 0.775 and 1.00. Based on the SEM and FlFFF data, $<r^2>_p^{1/2}$ would lie between 32 and 33 nm if the hematite particles were perfect solid spheres. This is unlikely, however. The particles are not perfectly spherical and they may have internal voids. In addition, the refractive index of hematite is 3.0 [26], which violates the Raleigh-Gans assumption that $\eta - \eta_0 < 1$. Given these limitations, the agreement of the MALS data with FlFFF using UV detection and with SEM is quite good. In fact, the combination of MALS with FlFFF yields more accurate polydispersity information compared to FlFFF without MALS, as indicated by the standard deviation in $<r^2>^{1/2}$ of 6 nm, which is close to the value (5 nm) obtained by measuring individual particles with SEM.

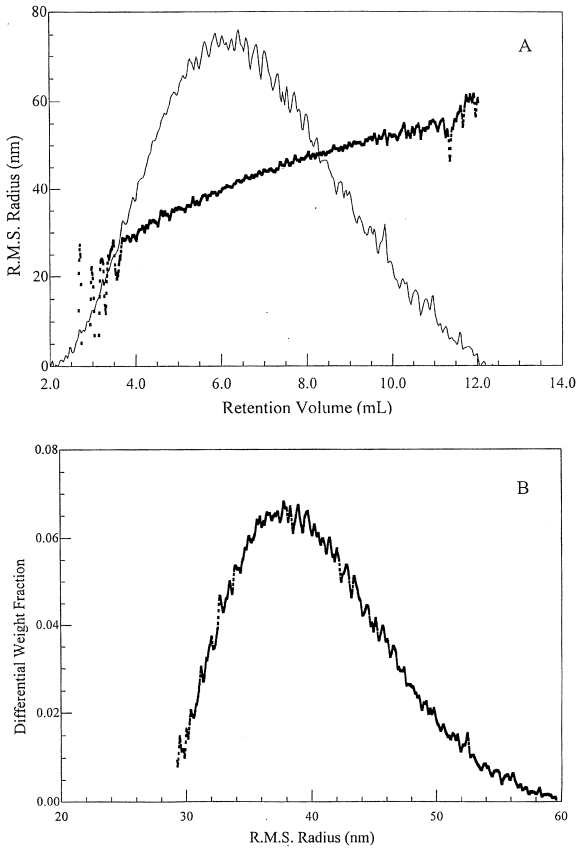

Fig. 3. Characterization of hematite by FlFFF/MALS: (A) overlay of the root-mean-square (R.M.S.) radius across the elution profile; (B) resulting weight-fraction size distribution.

In our study of the adsorption of humic and fulvic acid to hematite, we avoided the use of FL-70 and NaN_3, which are expected to affect both the conformation of the acids in solution (particularly humic acids, which are larger molecules) and their interaction with hematite. Without a surfactant in the carrier liquid, the elution profile for hematite changes slightly. The peak remains in the same position, but a broad tail appears. In Fig. 4 the size distribution of hematite obtained from instrument A is shown using DI water and retention theory to relate V_r to r_h. Like that obtained with FL-70 (Fig. 2), the distribution obtained in DI water peaks at a radius of 41 nm. However, increased tailing in the distribution indicates the presence of aggregated particles. We note that there could also be aggregated particles in FL-70 (Fig. 2), in which case the aggregation is simply

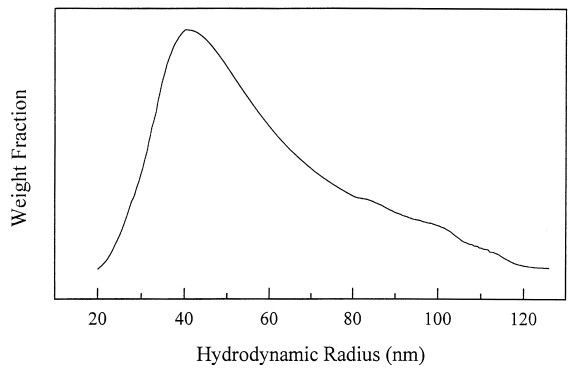

Fig. 4. Size distribution of hematite obtained by FlFFF using DI water as the carrier liquid and retention theory to relate retention time to hydrodynamic radius.

more pronounced in DI water. Either way, the presence of aggregated material is undesirable, which is why a surfactant is commonly used when characterizing particles by FFF. Fortunately, the increased tailing of the distribution in DI water is not great, and therefore not a cause for concern in the adsorption studies.

3.2. Adsorption of acids to hematite

In Fig. 5 an overlay of elution profiles obtained in DI water with separate injections of hematite (750 μg/ml) is shown, the humic acid SPHA (500 μg/ml), and a mixture of the two materials. By setting the detector wavelength to 280 nm, the signal for hematite is much smaller than that for SPHA. To illustrate the difference, Fig. 5 contains elution profiles for hematite obtained with two different detector sensitivities. When the sensitivity is set to a value equal to that used for observing the elution profiles of pure SPHA, the hematite signal is barely visible above the baseline. In order to obtain a comparable signal for hematite, the detector sensitivity must be increased by a factor of 50.

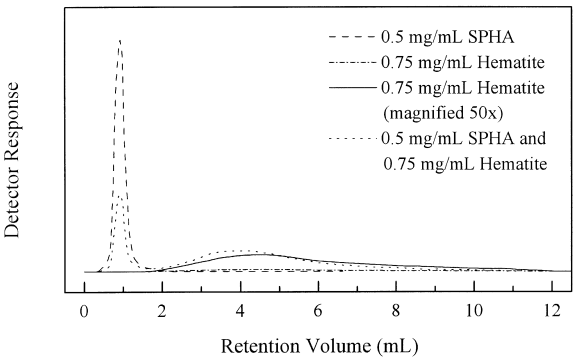

Fig. 5. Overlay of FlFFF elution profiles for bare hematite, Sphagnum peat humic acid (SPHA), and a mixture of the two. The mixture was allowed to equilibrate for 5 days prior to analysis.

Note that the elution profile of bare hematite is shifted to higher retention volumes compared to profiles obtained in 0.05 wt% FL-70 (see Fig. 2A). The shift is due to an increase in the void volume from 0.70 ml to 0.90 ml when FL-70 is absent from carrier liquid. The increase in V^0 was confirmed by the injection of several low molecular weight materials, which are not retained with the flow conditions used in this work.

Consider the elution profile of the mixture of SPHA and hematite displayed in Fig. 5. The first peak, which elutes in the void volume, represents SPHA that is not adsorbed to hematite at the time of injection. It elutes in the void volume because the field is not strong enough to overcome its rapid diffusion, which is required to concentrate it in the slower moving flow streams near the accumulation wall. The second more-retained peak does not represent hematite (which gives a barely detectable signal at the detector sensitivity used in this experiment), but rather SPHA that is adsorbed to hematite.

After the complex has been injected and the stop-flow period completed (i.e. elution has commenced), any free acid rapidly moves ahead of the hematite particles because such material it is not affected by the field. As the concentration of free acid in the solution immediately surrounding the hematite particles is reduced to zero, acid will begin to desorb from the hematite if the adsorption is reversible. As desorbed acid diffuses through the zone of hematite toward the center of the channel, it may adsorb and desorb several times, but eventually it will move ahead of the slower moving hematite. Consequently, the retention time of acid that is adsorbed to hematite at the time of injection will lie somewhere between the void time and the retention time of bare hematite.

The evidence regarding reversibility in the adsorption of acid to iron particles is unclear. In some reports [26], reversibility is evidenced by Langmuir-type isotherms, but in others [27] the reversibility of

adsorption is questionable. Reversibility not only depends on the pH and ionic strength of the surrounding environment, but it appears to change with equilibration time (i.e. the time between mixing and analysis of the adsorption complex). The fact that adsorbed acid elutes ahead of hematite suggests that its adsorption to hematite is, in fact, reversible in DI water. However, we must consider an alternate explanation, namely that coated hematite is repelled from the accumulation wall into faster moving flowstreams. Cases of decreased particle retention due to wall repulsion are well-documented in the FFF literature [28,29]. Thus, desorption is not necessarily responsible for the early elution of acid that is adsorbed to hematite at the time of injection. This issue is considered further below.

The retention ratio of acid that is adsorbed to hematite at the time of injection can be related to the fraction of time (t_a/t_r) that it spends in an adsorbed state during its migration through the channel:

$$R_a = \frac{t_0}{t_r} = 1 - \frac{t_a}{t_r}(1 - R_e) \quad (8)$$

Here R_a is the retention ratio of the acid (or other adsorbate) and R_e is the retention ratio of the hematite (or other adsorbent). More stable adsorption complexes will have larger values of t_a and therefore be retained longer in the channel (smaller R_a).

In Fig. 6 the retention volume associated with the retained-peak maximum ($V_{r,p}$) are plotted versus equilibration time for mixtures containing 750 μg/ml hematite and 500 μg/ml acid. For both humic and fulvic acids, $V_{r,p}$ increases with equilibration time, indicating that either the stability of the complex increases or wall repulsion decreases with time. Note that with fulvic acid, $V_{r,p}$ reaches a plateau value within a few hours, whereas $V_{r,p}$ for humic acid continues to increase for several days until it matches that of hematite. Whether the shift in $V_{r,p}$ with time is due to an increase in complex stability or a decrease in wall repulsion, the fact that it occurs over a wide range of equilibration times with humic acid suggests that rearrangements in molecular conformation occur after adsorption, as proposed in independent reports by Murphy [4] and Wershaw [26].

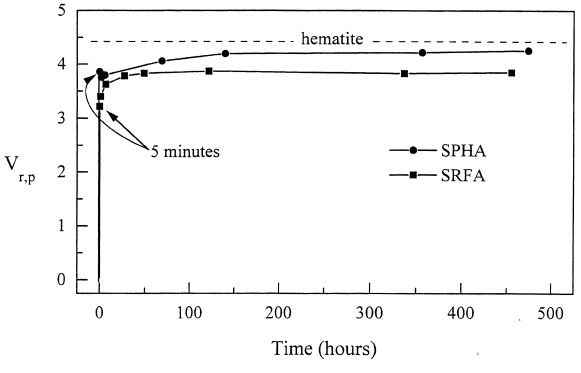

Fig. 6. Peak retention volume ($V_{r,p}$) versus equilibration time for mixtures containing 750 μg/ml hematite and 500 μg/ml of either Sphagnum peat humic acid (SPHA) or Suwannee River fulvic acid (SRFA).

In an effort to further examine the issue of complex stability versus wall repulsion as the mechanism responsible for the shift in $V_{r,p}$, we collected a 1-ml fraction early in the retained peak of several experiments, spun the fractions down in a microcentrifuge, and measured the UV absorbance of the supernatants at 280 nm. When the equilibration time was small, we measured a significant amount of absorbance, indicating the presence of desorbed acid. In the case of the humic acid, however, the UV absorbance decreased with equilibration time; when the equilibration time was greater than 100 h, the absorbance was negligible. For the fulvic acid experiments, the absorbance of the supernatant was not only higher compared to humic acid, but remained high regardless of equilibration time. Thus, a decrease in UV absorbance correlates with an increase in $V_{r,p}$, which supports our view that at least some desorption of acid occurs during the FlFFF experiment. However, the correlation does not prove that the shift in $V_{r,p}$ with equilibration time is due to desorption rather than ionic repulsion of coated hematite from the accumulation wall.

In the next set of experiments, we prepared a series of mixtures containing 750 μg/ml hematite and various concentrations of acid. Based on the previous results, we allowed these mixtures to equilibrate for one week prior to analysis by FlFFF. In Fig. 7 the elution profiles obtained using humic concentrations of 30 and 500 μg/ml are compared. The effect of concentration on the elution profile differs significantly among the two acids. The complexed fulvic acid continues to elute well ahead of hematite, regardless of its concentration in the mixture. By

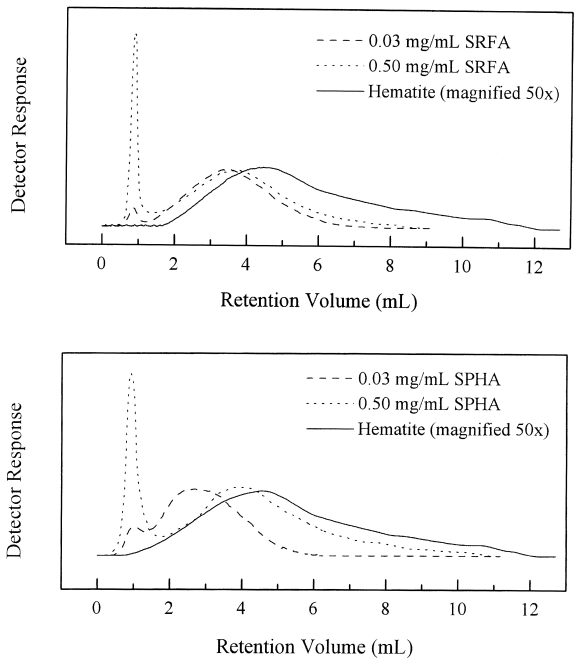

Fig. 7. Overlay of FlFFF elution profiles for bare hematite and mixtures containing hematite and either low or high concentrations of acid.

contrast, retention of adsorbed humic acid increases with concentration, and at a concentration of 0.5 mg/ml, nearly matched that of bare hematite.

In Fig. 8 the dependence of $V_{r,p}$ on the concentration of acid over a concentration range of 8–2000 μg/ml is shown. With the fulvic acid, $V_{r,p}$ increases sharply from 0–60 μg/ml. In this range, the void peak is small or non-existent, which indicates that fulvic acid is completely adsorbed at the

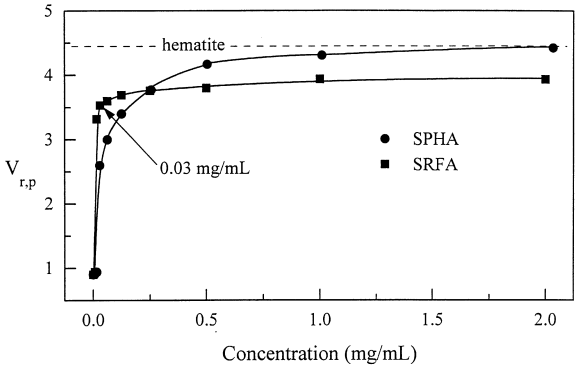

Fig. 8. Peak retention volume ($V_{r,p}$) versus concentration of acids.

time of injection. However, the poor retention compared to bare hematite suggests that there is either a large amount of wall repulsion or that a significant amount of desorption occurs during the separation. Above a concentration of 60 μg/ml, the size of the void peak continues to increase with concentration, and $V_{r,p}$ reaches a plateau value that remains much lower than that of bare hematite. This behavior indicates that the adsorption sites on the hematite become saturated at a fulvic acid concentration of 60 μg/ml. By contrast, $V_{r,p}$ for the humic acid continues to increase with concentration until it matches that of bare hematite.

For characterizing adsorption complexes that are reversible, FFF with secondary chemical equilibria can in principle be used to obtain the adsorption coefficients. However, this was not an option here since the continuous infusion of hematite would quickly destroy the channel membrane. An alternative method for obtaining adsorption isotherms is to quantify the amount of material adsorbed at the time of injection using peak areas in the elution profile. Unfortunately, the amount of adsorbed material cannot be obtained directly from the retained peak because we have no simple way of determining the dependence of the detector signal on acid concentration, that is we have no way of determining the extinction coefficient of the adsorbed acids. We can, however, measure the extinction coefficient of the free acids. Using the extinction coefficients, we can calculate the amount of free acid at the time of injection from the area of the void peak. From the total amount of injected acid and the calculated amount of free acid, we can back-calculate the amount of adsorbed acid. In Fig. 9 plots of void-peak areas versus mass of acid injected in the absence of hematite for both SPHA and SRFA are shown. The lines in the plot represent a linear least-squares fit of the data forced through the origin; the slopes equal the extinction coefficients.

Using this method, we calculated the mass of free acid for most of the mixtures represented in Fig. 8. (Those mixtures that yielded a $V_{r,p}$ value less than 2.5 ml were omitted because of poor resolution between the adsorbed and free material.) By subtracting the mass of free acid from the injected mass, we obtained the amount of acid adsorbed to hematite at the time of injection. We note that this method does

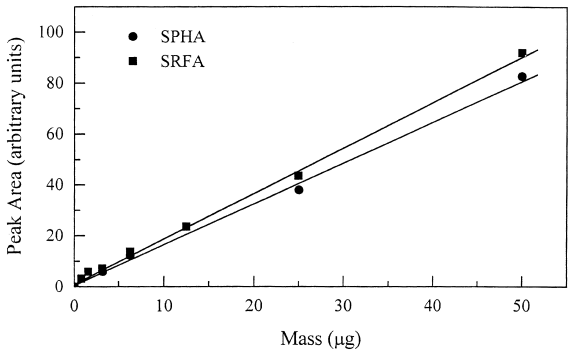

Fig. 9. Calibration plot of peak area versus mass of acid.

not rely on complete recovery of the adsorbed acid, which would be reduced by adsorption of hematite to the membrane. Even if some of the free acid is lost, the method is valid if recovery of acid that is free at the time of injection is independent of the presence of the hematite. The method also assumes that acid is not desorbed during the stop-flow period, so that the void peak contains only material that was not adsorbed to hematite at the time of injection. Although this assumption may not be strictly valid, we believe any associated error is small since the void peak continues to decrease with the concentration of acid, and never levels off at some finite concentration. In fact, we minimized the stop-flow time for this reason. Thus, the stop-flow time was chosen to be long enough that the retained peak is resolved from the void peak for all but the smallest acid concentrations, but short enough to be a small fraction of the time required to elute the adsorbed acid. We note that the stop-flow time was the same for all experiments, so that any error associated with this assumption will not affect the shape of the resulting isotherms.

The isotherms are illustrated in Fig. 10. The adsorption of humic acid continues to increase with concentration up to 2000 μg/ml. This behavior is consistent with that of a peat humic acid reported by Murphy et al. [4]. The large amount of adsorption combined with the shape of the isotherm is strong evidence for the formation of multiple adsorption layers. We note that even though the adsorption of humic acid continues to increase with concentration up to 2000 μg/ml, further increases were limited by the solubility of the humic acid. By contrast, the

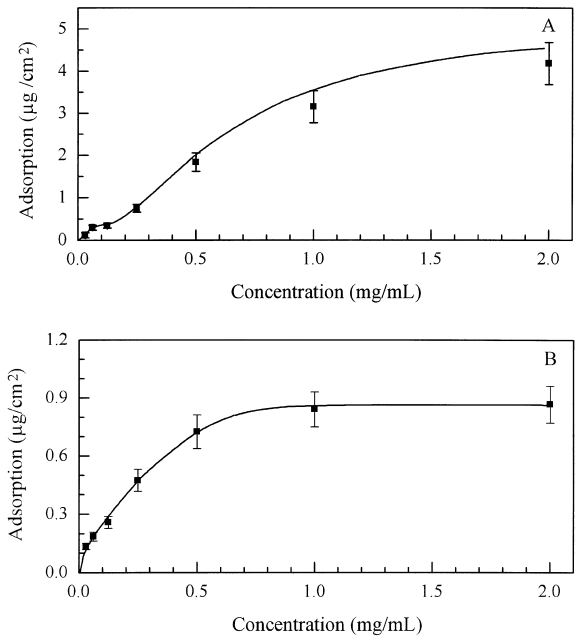

Fig. 10. Adsorption isotherms for (A) Sphagnum peat humic acid (SPHA), and (B) Suwannee River fulvic acid (SRFA).

fulvic acid exhibits Langmuir-type behavior, indicating monolayer adsorption.

To estimate the surface density associated with a monolayer of acid on hematite, we assume that the hematite particles are spherical with an average diameter of 85 nm and a specific gravity of 5.24 [30]. Based on the peak molecular weight and hydrodynamic diameter of the acids (Table 1), we estimate that a monolayer of fulvic acid would contain 0.2 $\mu g/cm^2$, while a monolayer of humic acid would contain <0.1 $\mu g/cm^2$. Of course, these are very crude estimates, which assume a spherically coiled molecule on the surface. The true values could be greater or less depending on the molecular conformation of the adsorbed molecules and whether or not they lie flat on the surface.

Referring to Fig. 10, the isotherm for fulvic acid plateaus at about 0.8 μg of acid per cm^2 of hematite. For humic acid, on the other hand, adsorption continues to increase even above a surface density of 4 μg per cm^2. It is apparent, therefore, that humic acid forms multiple adsorption layers, while fulvic acid forms only a few layers at most. This is not surprising given the fact that the humic acid mole-

cules tend to form large aggregates when concentrated in solution, whereas fulvic acids aggregate little if at all [8,15]. As multiple layers of humic acid adsorb and aggregate, the complex would also be expected to stabilize, as the data in Fig. 8 suggests. Thus, $V_{r,p}$ for the humic acid complex reaches that of bare hematite as the humic acid concentration is increased, whereas $V_{r,p}$ for the fulvic acid complex changes little with concentration and never reaches that of bare hematite.

4. Conclusions

FlFFF shows promise as a tool for studying the adsorption of acids to environmental colloids. Information on the rate of adsorption can be obtained by monitoring changes in the elution profile of adsorption complexes over time. In this work, for example, we found that the adsorption of both humic and fulvic acids to hematite occurs within a few minutes of combining the materials. If we assume that desorption and not wall repulsion is responsible for the shifts in retention with equilibration time, then we can further conclude that humic acid forms a more stable complex than fulvic acid. If wall repulsion is responsible for the shift in retention with equilibration time, then some sort of molecular rearrangement of adsorbed molecules must occur. Either mechanism can be supported by the current literature, and it may be possible to resolve the ambiguity by comparing the shift in retention with different membrane materials since repulsion effects are expected to vary with membrane composition.

Thermodynamic information in the form of adsorption isotherms can be obtained when the following conditions are met: (1) material that is complexed at the time of injection into the FlFFF channel can be separated from free material; (2) the recovery of free material is either complete or unaffected by presence of the adsorbent; (3) Significant desorption does not occur during stop-flow relaxation. The last requirement could prove to be the greatest limiting factor in expanding the method to other complexes, particularly those with smaller adsorption coefficients.

The isotherms produced in this study indicate that hematite has a greater adsorption capacity for humic acid compared to fulvic acid. The difference in capacity cannot be explained by differences in molecular size. Both the quantity of material adsorbed and the shape of the isotherm indicate that humic acid forms multiple adsorption layers. This behavior is in contrast to fulvic acid, where monolayer adsorption is indicated.

For studying adsorption phenomena, FlFFF has several advantages compared to the traditional method of centrifugation. Perhaps the greatest of these is the speed at which the free and complexed material can be separated. FlFFF also avoids partial remixing of the separated materials, which occurs in centrifugation when the field is relaxed in order to collect and quantify the materials. A third advantage of the FlFFF method is that only milligram quantities of material are required, an important consideration for the study of materials that require long and tedious purification methods.

A secondary aspect of the study presented here regards the measurement of size distributions of colloidal material by FlFFF. Although the mean size obtained by FlFFF agrees well with those obtained by SEM, the polydispersity of the sample is overestimated due to band broadening in the separation process. Unfortunately, band broadening is not as well-defined for FlFFF compared to other FFF subtechniques due to the roughness of the channel membrane. However, by combining FlFFF with MALS, detailed size distributions are obtained with greater precision than possible with either technique alone.

Acknowledgements

We wish to thank Dr. Robert Wershaw for providing the humic acid sample, Wyatt Technology for the use of their MALS instrument, and Dr. Karin Caldwell for her consultations. This work was funded by Grant CHE-9634195 from the National Science Foundation and Grant R821828-01-0 from the Environmental Protection agency.

References

[1] D.C. Nayak, C. Varadachari, K. Ghosh, Soil Sci. 149 (1990) 268–271.

[2] E. Tipping, Geochim. Cosmochim. Acta 45 (1981) 191–199.
[3] C. Varadachari, T. Chattopadhyay, K. Ghosh, Soil Sci. 162 (1997) 28–34.
[4] E.M. Murphy, J.M. Zachara, S.C. Smith, J.L. Phillips, T.W. Wietsma, Environ. Sci. Technol. 28 (1994) 1291–1299.
[5] R.R. Engebretson, R. von Wandruszka, Environ. Sci. Technol. 28 (1994) 1934–1941.
[6] M. Grätzel, J.K. Thomas, J. Am. Chem. Soc. 95 (1973) 6885–6889.
[7] E.A. Lissi, E.B. Abuin, L. Sepulveda, J.H. Quina, J. Phys. Chem. 88 (1984) 81–85.
[8] M.P. Petteys, M.E. Schimpf, Coll. Surf. 120 (1997) 87–100.
[9] A. Berthod, D.W. Armstrong, Anal. Chem. 59 (1987) 2410–2413.
[10] S. Terabe, S.K. Otsuka, K. Ichikawa, A. Tsuchiya, T. Ando, Anal. Chem. 56 (1984) 111.
[11] M. Hoyos, M. Martin, Anal. Chem. 67 (1995) 1179–1185.
[12] A. Berthod, D.W. Armstrong, M.N. Myers, J.C. Giddings, Anal. Chem. 60 (1988) 2138–2141.
[13] J.T. Li, K.D. Caldwell, J. Chromatogr. 555 (1991) 260–266.
[14] R. Beckett, J. Ho, Y. Jiang, J.C. Giddings, Langmuir 7 (1991) 2040–2047.
[15] M.E. Schimpf, K.-G. Wahlund, J. Microcol. Sep. 9 (1997) 535–543.
[16] R. Beckett, Z. Jue, J.C. Giddings, Environ. Sci. Technol. 21 (1987) 289–295.
[17] E. Matijevic, P. Scheiner, J. Coll. Interf. Sci. 63 (1978) 509–524.
[18] N.H.G. Penners, L.K. Koopal, Coll. Surf. 19 (1986) 337–349.
[19] M.E. Schimpf, Ind. J. Techn. 31 (1993) 443–457.
[20] S.K. Ratanathanawongs, I. Lee, J.C. Giddings, in: T. Provder (Editor), Particle Size Distribution II, ACS Symposium Series 472, American Chemical Society, Washington, D.C., 1991, Chapter 15, pp. 229–246.
[21] H.C. van de Hulst, in: Light Scattering by Small Particles, Dover Publications, New York, 1981.
[22] P. Reschiglian, D. Melucci, A. Zattoni, G. Torsi, J. Microcol. Sep. 9 (1997) 545–556.
[23] R. Beckett, T.T. Hart, in: F. Buffle, H.P. van Leeuwen (Editors), Environmental Particles, vol. 2, Lewis Publishers, Ann Arbor, 1993, Chapter 4, pp. 165–205.
[24] P.J. Wyatt, Anal. Chim. Acta 272 (1993) 1–40.
[25] H. Thielking, D. Roessner, W.-M. Kulicke, Anal. Chem. 47 (1995) 3229–3233.
[26] E. Tipping, Chem. Geology 33 (1981) 81–89.
[27] R.L. Wershaw, J.A. Leenheer, R.P. Sperline, Y. Song, L.A. Noll, R.L. Melven, G.P. Rigatti, Coll. Surf. 96 (1995) 93–104.
[28] M.E. Hansen, J.C. Giddings, R. Beckett, J. Coll. Inter. Sci. 132 (1989) 300–312.
[29] P.S. Williams, Y. Xu, P. Reschliglian, J.C. Giddings, Anal. Chem. 69 (1997) 349–360.
[30] CRC Handbook of Chemistry and Physics, 57th Ed., CRC Press, Cleveland, Ohio, 1976.